IEEE Access
Multidisciplinary | Rapid Review | Open Access Journal

Received April 6, 2020, accepted April 26, 2020, date of publication May 6, 2020, date of current version May 29, 2020.

Digital Object Identifier 10.1109/ACCESS.2020.2992780

Constant Power Load Stabilization in DC Microgrid Systems Using Passivity-Based Control With Nonlinear Disturbance Observer

MUSTAFA ALRAYAH HASSAN[1,2], **(Member, IEEE), AND YIGANG HE**[1]
[1]School of Electrical Engineering and Automation, Wuhan University, Wuhan 430072, China
[2]Department of Electrical Engineering, University of Blue Nile, Damazeen 26613, Sudan

Corresponding author: Yigang He (18655136887@163.com)

This work was supported in part by the National Natural Science Foundation of China under Grant 5197715351577046, in part by the State Key Program of National Natural Science Foundation of China under Grant 51637004, in part by the National Key Research and Development Plan ''important scientific instruments and equipment development'' under Grant 2016YFF0102200, and in part by the Equipment Research Project in advance under Grant 41402040301.

ABSTRACT This paper aims to present a robust passivity-based control (PBC) strategy to solve the instability problem caused by the constant power loads (CPLs) in dc microgrid systems. This strategy is designed to stabilize and regulate the dc-bus voltage of the dc microgrid and to eliminate the dc-bus voltage deviations caused by the system disturbances such as load and input voltage variations. To this end, the control robustness of the PBC strategy is improved by adding the nonlinear disturbance observer (NDO). Whereas, the PBC is applied to damp the system oscillation caused by the CPLs and to ensure that each parallel subsystem in dc microgrid is passive (stable). Based on estimation technique, the NDO works in parallel with the PBC strategy to compensate the system disturbances through a feed-forward compensation channels. Furthermore, the PBC strategy provides self-(*I*-*V*) droop characteristics, which able to eliminate the voltage mismatch between the parallel converters and obtain equal current sharing between them. This control strategy ensures large-signal stability, globally asymptotically stabilization and reacts extremely fast against system disturbances as compared with other PBC strategies. The MATLAB simulation and hardware-in-loop (HIL) experimental results are presented to verify the control robustness of the proposed controller.

INDEX TERMS Constant power load (CPL), dc microgrid, dc-dc power converter, passivity-based control (PBC), nonlinear disturbance observer (NDO), hardware-in-loop (HIL).

I. INTRODUCTION

With the development of the dc-distributed generation (DG) systems based on the renewable resources and fast growing of dc loads, the dc microgrids are becoming an effective alternative networks compared with the traditional ac-networks [1]–[3]. Fig.1 shows a typical system structure of the dc-microgrids with parallel source converters supplying parallel dc-loads through a common dc-bus. The dc-loads contain the constant voltage load (CVL) and CPLs. The parallel operation of dc-dc power converters in dc microgrid is necessary to increase system reliability, flexibility, and reduces the power stress on every single converter [4]. However, the main reason that destabilizes the dc-bus voltage of the dc microgrid is the tightly regulated point of load (POL) converters which behave as CPLs. This kind of loads have instability impact due its negative incremental impedance (NII). This impedance reduces the damping of the system with the loss-less energy dissipation across the source converters output terminals [5], [6]. Therefore, the energy of source-subsystems tends to oscillate internally between the inductor and capacitor circuits of the source converters, creating a limit cycle behavior [7]. This behavior increases the switching stress on source converters and makes the dc-bus voltage be unstable.

To solve the instability problem of the CPL, two linear and nonlinear control methods have been introduced in literature. The linear control method based small-signal model was presented by splitting the dc-network into two systems (source-subsystem and load-subsystem). The oscillation caused by

The associate editor coordinating the review of this manuscript and approving it for publication was Ning Sun.

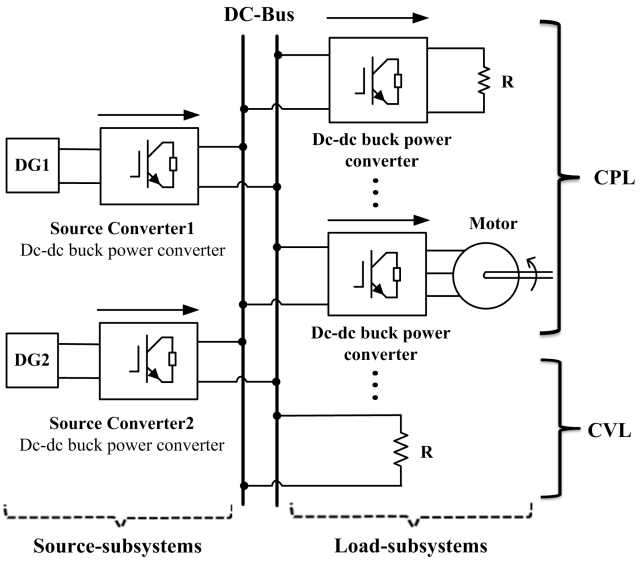

FIGURE 1. A typical structure of the dc microgrids.

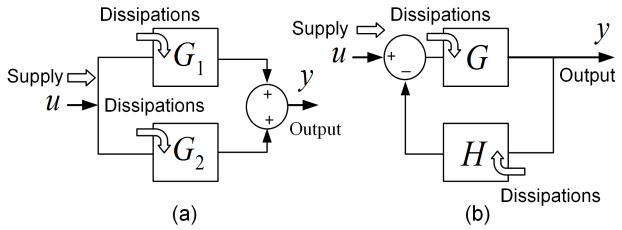

FIGURE 2. Passivity of combined system, (a) passivity of parallel-connected system, (b) passivity of feedback control system.

the CPLs is damped by adjusting the minor-loop gain of the dc-network (i.e the impedance ratio between source and load-subsystems) [8]. The condition of stability is satisfied if only if the Nyquist contour of the minor-loop gain does not encircle various forbidden regions including $(-1, 0)$ point [9]–[12]. In this regard, two different liner control techniques were implemented including; passive damping techniques by adding real damping elements [13], [14], or active damping techniques through control action [15]–[18]. For either techniques, the linear control method based impedance ratio can only provide an accurate control performance in small neighborhood to the equilibrium point. A typical control dynamics away from this point cannot be obtained [4], [5]. Therefore, numerous nonlinear control strategies based large-signal model are then introduced, such as sliding mode control (SMC) [19], model predictive control (MPC) [20], backstepping control [21], [22], synergetic control [23], and passivity-based control (PBC) [7]. The global stabilization condition of the dc microgrid can be achieved, as long as each parallel subsystem complied by self-disciplined stability [24]. Therefore, unlike other nonlinear control strategies, the PBC offers an effective theoretical tool to realize the concept of the energy dissipation. Using Euler-Lagrange equations, the passivity-based controller able to reshape the energy dissipation of system virtually through damping resistances injection, which lead to damp the system oscillation. An important feature provided by the PBC is that, if a group of passive subsystems are interconnected together through parallel or feedback connection, the resulted system is also passive (stable) [25], [26]. The intuitive reason is that, the energy supplied to the interconnected system is dissipated separately by each individual subsystem, as illustrated in Fig.2. Therefore, the stability target can be easily localized to every single converter, that facilitates the stability analysis for the entire dc microgrid system [24]. The application of the PBC strategy in power electronic converters was originally proposed by Ortega *et al.* [26], and followed by several scholars [27]–[34]. In [28], [35], the PBC scheme is developed to stabilize the CPLs in dc microgrids using a simple and effective liner proportional-derivative (PD) controller. However the main drawback of this controller is that it cannot eliminate the deviation (steady-state error) of the dc-bus voltage caused by the system disturbances such as line and load variations. To overcome this drawback, the complementary proportional integral derivative (PID) controller based on the parallel-damped PBC (PD-PBC) strategy is implemented by adding the PID controller [29]. In [30], the passivity-based integral control (PBIC) is also proposed to regulate the output voltage of the dc-dc boost power converter feeding resistive load. The addition of the integral gain is implemented to ensure both; global stability and control robustness against system uncertainties. Both previous control strategies (PD-PBC and PBIC) [29], [30], were implemented to control the dc-dc boost power converter supplying only a resistive load. The PBC strategy based an interconnected and damping assignment (IDA-PBC) is then proposed to control the DC-DC boost power converter feeding a CPL [31]. The IDA-PBC strategy is modeled based on a port-connected Hamiltonian system. The complementary proportional integral (PI) term is also added with the IDA-PBC to eliminated the steady-state error caused by the CPL. Due to the addition of the integral term to all previous PBC strategies, the steady-state error is completely removed. However, other performance issues emerged such as a high response overshoot, limited recovery performance and long settling time. The traditional PBC strategies combined with integral gain control such as PD-PBC, PBIC, and IDA-PBC [29]–[33], attenuate the system disturbance through feedback regulation rather than feedforward compensation control. Therefore, the control response of these strategies reacts in a relatively slow way at start-up and during disturbances. By applying higher integral gains, the control performance recovers faster, but the price is the higher maximum overshoot and long settling time. To avoid the weakness of previous PBC strategies, the NDO is applied to improve the control robustness through the feedforward control system rather than traditional feedback control with integral. The adaptive PBC using nonlinear disturbance observer (NDO) is proposed for a single dc-dc buck power converter feeding a CPL in dc microgrid systems [34], [36].

The NDO is applied as an effective key tool that can observe and estimate the disturbance of the system independently of the baseline controller (i.e. PBC). This observer operates in parallel with the PBC to compensate the disturbances of the system through a feed-forward compensation channel online with minimum information dynamics [37]–[40]. Recently the NDO observer emerged as an effective tools for disturbance rejection in many industrial applications including power electronics and generators control [41], [42]. An important feature offered by the NDO based feedforward compensation control is that, it can reject the disturbance of the system in faster way with extremely high recovery performance. Moreover, by adding the NDO, the nominal performance of the baseline controller can be easily recovered at the absence of disturbances. However, the adaptive PBC controller that presented in [36], is applied only for a single dc-dc source power converter feeding a CPL.

In this paper, the concept of adaptive PBC using NDO [36] has been extended for the dc-microgrid system level. Therefore, this paper aims to achieve the following three targets: (i) Stabilize and regulate the DC-bus voltage of the DC microgrid using PBC strategy, (ii) By combining the NDO to work in parallel with the PBC strategy, this paper also aims to eliminate the steady-state error caused by the system disturbances such as load and input voltage variations, and (iii) Eliminate the voltage mismatch between the parallel connected converters in DC microgrid using the self *I-V* droop control property of the PBC strategy. The dc micrgogrid contains parallel-connected dc-dc buck power converters feeding parallel-connected dc loads (CPL + CVL) through a common dc- bus (see Fig.1). The NDO is applied to improve control robustness of passivity-based controller by increasing the degree of control freedom, which makes the controller react very fast against system disturbances (line and load variation). Whereas, the PBC provides globally asymptotically stability for each individual source-subsystem by dissipating the energy oscillation caused by the CPL. In addition, this controller is presented to ensure both voltage regulation and equal current sharing between the parallel buck power converters locally without any communication. To this end, many *V-I* and *I-V* droop control methods have been introduced in literature [43]–[47]. The *V-I* droop regulates the dc-bus voltage depending on the output current of the parallel connected converters [43]–[45], whereas *I-V* droop controls the output current based on the dc-bus voltage [46], [47]. As compared with *V-I* droop control, the *I-V* droop control strategy provides faster dynamic response as well as best current sharing performance during large changing in the CPL [47]. The main feature provided by the PBC is that it has self-(*I-V*) droop characteristic which able to reshape the energy across output terminals of the parallel-connected dc-dc power converter through additional of virtual resistances. This virtual gain can eliminate the voltage mismatch between the parallel-connected converters through the control of the reference currents and equal current sharing to the CPL. All these features make the proposed control strategy (PBC with NDO) to be a successful control strategy for the application of DC microgrids systems. This control strategy is a nonlinear controller, provides large signal stability and ensures robust voltage control during system disturbance. To verify the control performance of the proposed controller, the MATLAB simulation results have been validated by means of hardware-in-loop (HIL) experimental platform using the OPAL-RT real-time simulator. The HIL platform allows the interconnection between the MATLAB simulation model (dc-dc buck power converters) and the real hardware controller [digital signal processor (DSP)] through the OPAL-RT real-time simulator. An important feature offered by the HIL system is a fact that the simulation model can work exactly in the same time scale as the real system would work.

The paper is organized as follows; Section II introduces the design of the PBC for the parallel-connected dc-dc buck power converters feeding a CPL. Section III presents the NDO design and the *I-V* droop control. The MATLAB simulation and HIL experiment results are presented in Section IV. The conclusion is drawn in Section V.

II. PASSIVITY-BASED CONTROL DESIGN FOR THE PARALLEL-CONNECTED DC-DC BUCK POWER CONVERTERS FEEDING A CPL

A. RELATIONSHIP BETWEEN PASSIVITY AND STABILITY IN DC MICROGRID SYSTEMS

The relationship between the passivity and the stability is earlier introduced by Youla *et al.* [48]. He proved that a passive network in closed-loop with a resistive element is $\mathcal{L}_2$ stable. In [49], it also proved that, the non-passive system can be transformed into passive system through passive feedback control system. The concept of the passivity describes the natural physics of nonlinear systems containing input ($u \in \mathbb{R}^n$) and output ($y \in \mathbb{R}^m$). The linear resistance-inductance-capacitance (RLC) circuit is a simple example to represent the passive system. The system is said to be passive if the energy injected by the external source $u^T y$ is always greater than the energy stored in the system $\dot{\mathcal{S}}(\tilde{z})$, with difference being the dissipated energy $\mathcal{Z}^T \mathcal{R}_i(z)\mathcal{Z}$. This intuitively means that, part of energy is dissipated by the system resistance and the rest of energy should have delivered to the system storage (capacitor and inductor). The passive system can be described by the following energy balance equation

$$\underbrace{\mathcal{S}(z(t)) - \mathcal{S}(z(0))}_{\text{stored energy}} + \underbrace{\int_0^t \mathcal{Z}^T \mathcal{R}_i(z)\mathcal{Z}dt}_{\text{dissipated energy}} = \underbrace{\int_0^t u^T(t)y(t)dt}_{\text{supplied energy}} \tag{1}$$

A passive system is considered as stable system because the energy dissipation function always driving the systems state $z(t)$ back towards the equilibrium point. In general, the DC microgrids contain parallel source-subsystems supplying other parallel load-subsystems through dc-dc power converters, as illustrated in Fig.1. Every single converter has

a local closed-loop feedback control system with various control parameter and different circuit parameters (inductors, capacitors, switches, and wires). This diversity add more challenges to analyze the nonlinear stability for the entire dc-microgrid, which may need a complicated dynamical equations. As long as the goal of this work is to solve the instability problem caused by CPLs, the stability analysis based on the passivity property can be easily obtained individually for each subsystem. This can be achieved by reshaping the energy of each subsystem to be strictly passive using passivity-based feedback controller (PBC). An important feature provided by the PBC is that, if two group of passive subsystems are interconnected together through parallel or feedback connection, the resulted system is also passive (stable) (see Fig.2) [24]. This is implies that, the energy supplied by each source-subsystems would have dissipated by the other load subsystem. In this sense, the overall energy balance of the dc-microgrid is always positive.

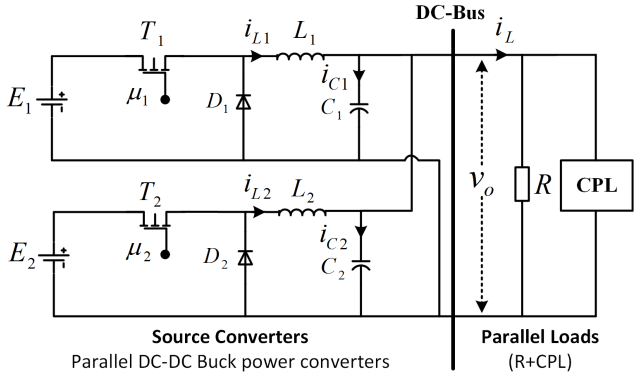

FIGURE 3. DC microgrid structure with dc-dc buck power converters feeding a CPL and CVL.

B. PROBLEM FORMULATION AND EQUATIONS MODELING

Fig.3 depicts the electrical circuit diagram of the DC microgrid contain parallel dc-dc buck power converters feeding parallel dc loads [purely resistive (R) load and CPL]. The parameters of the dc-dc buck power converters are denoted as follows; (E_1, E_2), (L_1, L_2) and (C_1, C_2) represent the input voltages, the inductances, and the capacitances of the parallel circuits respectively. Whereas (i_{L1}, i_{L2}), (v_o) and ($\mu_1, \mu_2 \in [0, 1]$) represent the inductor currents, the output voltage and the duty ratios of the parallel system respectively. The entire parallel system (source and load power converters) are assumed to be working in continuous conduction mode (CCM). The dynamic equations of the parallel combination are written as:

$$\begin{cases} \dot{i}_{L1} = \dfrac{E_1}{L_1}\mu_1 - \dfrac{v_o}{L_1}, \\ \dot{i}_{L2} = \dfrac{E_2}{L_2}\mu_2 - \dfrac{v_o}{L_2}, \\ \dot{v}_o = \dfrac{i_{L1}}{C_{eq}} + \dfrac{i_{L2}}{C_{eq}} - \dfrac{v_o}{C_{eq}R} - \dfrac{P}{C_{eq}v_o}. \end{cases} \tag{2}$$

To address the instability problem of the dc microgrid caused by the CPLs, all damping elements (i.e. parasitic components and line resistances) have been neglected. The disturbances of the system caused by the line and load variation and the uncertainty due to parameters variation are included to (2) as follows:

$$\begin{cases} \dot{i}_{L1} = \dfrac{E_{1o}}{L_{1o}}\mu_1 - \dfrac{v_o}{L_{1o}} + d_1, \\ \dot{i}_{L2} = \dfrac{E_{2o}}{L_{2o}}\mu_2 - \dfrac{v_o}{L_{2o}} + d_2, \\ \dot{v}_o = \dfrac{i_{L1}}{C_{eqo}} + \dfrac{i_{L2}}{C_{eqo}} - \dfrac{v_o}{C_{eqo}R_o} - \dfrac{P_o}{C_{eq}v_o} + d_3. \end{cases} \tag{3}$$

where (d_1, d_2): represent the disturbances/uncertainties of system due to input voltage changes as well as parameter variations of the inductances (L_1, L_2).

$$d_1 = \frac{E_1}{L_1}\mu_1 - \frac{E_{1o}}{L_{1o}}\mu_1 + \frac{v_o}{L_{1o}} - \frac{v_o}{L_1}. \tag{4}$$

$$d_2 = \frac{E_2}{L_2}\mu_2 - \frac{E_{2o}}{L_{2o}}\mu_2 + \frac{v_o}{L_{2o}} - \frac{v_o}{L_2}. \tag{5}$$

and d_3: is the disturbance/uncertainty of the parallel converters due to the load changes and capacitor variations.

$$d_3 = \frac{i_{L1}}{C_{eq}} - \frac{i_{L1}}{C_{eqo}} + \frac{i_{L2}}{C_{eq}} - \frac{i_{L2}}{C_{eqo}} + \frac{v_o}{C_{eqo}R_o} - \frac{v_o}{C_{eq}R} + \frac{P_o}{C_{eqo}v_o} - \frac{P}{C_{eq}v_o}. \tag{6}$$

where (L_{1o}, L_{2o}), (E_{1o}, E_{2o}), C_{eqo} and R_o represent the nominal values of (L_1, L_2), (E_1, E_2), C_{eq} and R respectively. Defining:

$$\mathcal{Z} = \begin{pmatrix} z_1 \\ z_2 \\ z_3 \end{pmatrix} = \begin{pmatrix} i_{L1} \\ i_{L2} \\ v_o \end{pmatrix}, \quad \mathcal{H} = \begin{pmatrix} L_1 & 0 & 0 \\ 0 & L_2 & 0 \\ 0 & 0 & C_{eq} \end{pmatrix},$$

$$\Gamma = \begin{pmatrix} E_1 \\ E_2 \\ 0 \end{pmatrix}, \quad \mathcal{G} = \begin{pmatrix} 0 & 0 & 1 \\ 0 & 0 & 1 \\ -1 & -1 & 0 \end{pmatrix}, \text{ and}$$

$$\mathcal{R}(z) = \begin{pmatrix} 0 & 0 & 0 \\ 0 & 0 & 0 \\ 0 & 0 & \left(\dfrac{1}{R} + \dfrac{P}{z_3^2}\right) \end{pmatrix}.$$

For sake of simplicity, Equations (2) and (3) can be reformulated in matrices form as follows:

$$\mathcal{H}\dot{\mathcal{Z}} + [\mathcal{G} + \mathcal{R}(z)]\,\mathcal{Z} = \mu\Gamma. \tag{7}$$

$$\mathcal{H}_o\dot{\mathcal{Z}} + [\mathcal{G} + \mathcal{R}_o(z)]\,\mathcal{Z} = \mu\Gamma_o + d. \tag{8}$$

where $d = [\,d_1 \;\; d_2 \;\; d_3\,]^T$ is the disturbances vector of the system and $\mathcal{H}_o$, $\mathcal{R}_o(z)$ and $\mu\Gamma_o$: are the nominal matrices of the $\mathcal{H}$, $\mathcal{R}(z)$ and $\mu\Gamma$ respectively. This paper aims to achieve the following main goals; (i) stabilize and regulate the dc-bus voltage feeding the CPL. (ii) eliminate the dc-bus voltage deviations caused by the disturbances of the system (i.e. input voltage and load variations). To this end, the passivity-based control with nonlinear disturbance

observer is applied to achieve the following asymptotically stability condition;

$$\lim_{t\longrightarrow\infty}[\mathcal{Z}-\mathcal{Z}_d]=0,\quad \forall\,(z_{10}\geq 0, z_{20}\geq 0 \text{ and } z_{30}>\varepsilon). \quad (9)$$

where z_{10}, z_{20} and z_{30}: are the initial conditions of the system states, $\mathcal{Z}_d = \begin{bmatrix} z_{1d} & z_{2d} & z_{3d}\end{bmatrix}^T = \begin{bmatrix} I_{L1} & I_{L2} & V_o\end{bmatrix}^T$: is the vector of the desired equilibrium points, and ε is a small positive value.

C. PASSIVITY-BASED CONTROL

Basically, the passivity property for any electrical circuit is defined based on the balance between energy provided by the electrical sources and the sum of the energy dissipated plus the energy stored. Because the effect of the CPLs, the dc-bus voltage of the dc microgrid exhibits a limit cycle behavior. In fact, the NII of the CPL makes the system has less energy dissipation to damp the transient energy provide by the storage elements in the source converters circuits (i.e. the inductors and the capacitors). This is may leads the energy oscillation between the circuits of the inductors and capacitors. This problem was solved by adding real damping elements [13], [14]. However, this solution is energy consuming, which is considered as costly solution. To solve this problem, the effective virtual damping resistances can be applied by modifying the control action, which makes the parallel circuits of the source converters as containing series virtual resistances along the inductor circuits (R_{1d}, R_{2d}) and parallel virtual resistances across the output capacitors circuits R_{3d} (see Fig. 4) [28], [36]. To reshape the energy of the system virtually through the feedback control signals, the following two stages have to be followed.

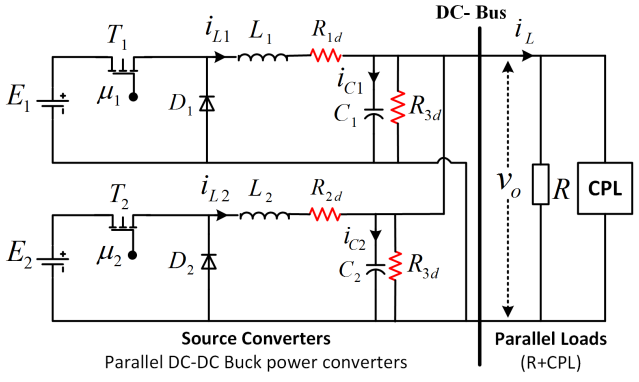

FIGURE 4. DC microgrid structure with adding the damping virtual resistances. R_{1d} and R_{2d}.

1) ENERGY SHAPING STAGE

As any power electronic converter contains energy stored circuits; i.e. potential energy in the capacitor circuit and kinetic energy in the inductor circuit. The energy shaping stage is important to reshape the coordinates of the stored energy by including the new deviation of both; potential and kinetic energy to achieve a unique minimum in the new desired equilibrium. Therefore, this stage is important to reshape the coordinates of (7) by including the state variables deviation ($\tilde{\mathcal{Z}}$) from the set point ($\mathcal{Z}_d$) as follows:

$$\mathcal{H}\dot{\tilde{\mathcal{Z}}}+[\mathcal{G}+\mathcal{R}(z)]\,\tilde{\mathcal{Z}}=\mu\Gamma-\left(\mathcal{H}\dot{\mathcal{Z}}_d+[\mathcal{G}+\mathcal{R}\,(z)]\,\mathcal{Z}_d\right) \quad (10)$$

2) DAMPING INJECTION STAGE

This stage is necessary to damp the energy oscillation of the system virtually by injecting the damping resistance matrix. This can be achieved by modifying the dissipation function virtually using the closed-loop feedback control system. The global stabilization can be achieved by reshaping the energy of the system through the closed-loop feedback controller to compensate the energy difference between the energy of the system and the energy injected by the controller. Therefore, the energy oscillation of the system can be damped virtually by injecting the damping resistance matrix ($\mathcal{R}_d\tilde{\mathcal{Z}}$) to both sides of (10):

$$\begin{aligned}\mathcal{H}\dot{\tilde{\mathcal{Z}}}+[\mathcal{G}+\mathcal{R}_i(z)]\,\tilde{\mathcal{Z}}&=\mu\Gamma\\&\quad-\left(\mathcal{H}\dot{\mathcal{Z}}_d+[\mathcal{G}+\mathcal{R}\,(z)]\,\mathcal{Z}_d-\mathcal{R}_d\tilde{\mathcal{Z}}\right)\end{aligned} \quad (11)$$

where:

$$\begin{cases}\mathcal{R}_i(z)=\begin{pmatrix}R_{1d} & 0 & 0\\ 0 & R_{2d} & 0\\ 0 & 0 & \left(\dfrac{1}{R_{3d}}+\dfrac{1}{R}+\dfrac{P}{z_3^2}\right)\end{pmatrix},\\ \mathcal{R}_d=\mathcal{R}_i(z)-\mathcal{R}(z)=\begin{pmatrix}R_{1d} & 0 & 0\\ 0 & R_{2d} & 0\\ 0 & 0 & \dfrac{1}{R_{3d}}\end{pmatrix}.\end{cases} \quad (12)$$

This is for all (R_{1d}, R_{2d}, and R_{3d}) >0

By injecting the virtual resistance matrix $\mathcal{R}_d$ which is also concurs with Lyapunov sense, the condition of global asymptotic stability can be guaranteed, as well as the transient energy of the system would be completely dissipated. Therefore, the left-hand side of (11) approach to zero as time going to infinity ($\tilde{\mathcal{Z}}=0$) [18], [27].

$$\mathcal{H}\dot{\tilde{\mathcal{Z}}}+[\mathcal{G}+\mathcal{R}_i(z)]\,\tilde{\mathcal{Z}}=0 \quad (13)$$

To prove (13), let us examine the stability of the proposed control strategy (PBC), by recalling the Lyapunov's stability criterion for the nonlinear systems [50]. Let $\tilde{z}=0$ the equilibrium point of the (13) and $\mathcal{D}\subset\mathbb{R}^m$ is the domain containing the $\tilde{z}=0$. Let $\mathcal{S}:\mathcal{D}\rightarrow\mathbb{R}$ be continuously differential function that

$$\mathcal{S}(0)=0 \quad \text{and } \mathcal{S}(\tilde{z})>0 \text{ in } \mathcal{D}-\{0\} \quad (14)$$

$$\dot{\mathcal{S}}(\tilde{z})\leq 0 \quad \text{in } \mathcal{D} \quad (15)$$

Then, the equilibrium point $\tilde{z}=0$ is stable. Moreover, if

$$\dot{\mathcal{S}}(\tilde{z})<0 \quad \text{in } \mathcal{D}-\{0\} \quad (16)$$

Then, equilibrium point $\tilde{z}=0$ is asymptotically stable.

Motivated by Lyapunov function candidate and the positive definite matrix $\mathcal{H}$, the total energy stored related to the stabilization error, can be written as

$$\mathcal{S}(\tilde{z}) = \frac{1}{2}\tilde{\mathcal{Z}}^T \mathcal{H}\tilde{\mathcal{Z}} > 0 \quad (\forall \tilde{\mathcal{Z}} \neq 0) \tag{17}$$

The transient dynamic of stored energy (17) can be written as:

$$\dot{\mathcal{S}}(\tilde{z}) = \tilde{\mathcal{Z}}^T \mathcal{H}\dot{\tilde{\mathcal{Z}}} \tag{18}$$

Equation (13) can be reformulated in the following form

$$\dot{\tilde{\mathcal{Z}}} = -\mathcal{H}^{-1}\left[\mathcal{G} + \mathcal{R}_i(z)\right]\tilde{\mathcal{Z}} \tag{19}$$

By Substituting (19) into (18), the result is

$$\dot{\mathcal{S}}(\tilde{z}) = -\left[\tilde{\mathcal{Z}}^T \mathcal{G}\tilde{\mathcal{Z}} + \tilde{\mathcal{Z}}^T \mathcal{R}_i(z)\tilde{\mathcal{Z}}\right] \tag{20}$$

Because $\mathcal{G}$ is a skew symmetric matrix [i.e. $(\mathcal{G} + \mathcal{G}^T = 0)$], therefore the part $\tilde{\mathcal{Z}}^T \mathcal{G}\tilde{\mathcal{Z}}$ in (20) is equal zero. Finally, the energy dynamics of $\mathcal{S}(\tilde{z})$ along the solution of (13) can be written as

$$\dot{\mathcal{S}}(\tilde{z}) = -\tilde{\mathcal{Z}}^T \mathcal{R}_i(z)\tilde{\mathcal{Z}} < 0 \tag{21}$$

From (21) we can notice that, the rate of energy stored is decreasing over the time which always considered as stable behavior. The energy stored $\mathcal{S}(\tilde{z})$ in the passive system place exactly the same rule as the Lyapunov function in the system without input. We can conclude that, the transient dynamic of stored energy is asymptotically approach to zero independently of the duty ratio μ [27], [36]. Thus, the right-hand side of (11) is written as

$$\mu\Gamma - \left(\mathcal{H}\dot{\mathcal{Z}}_d + \left[\mathcal{G} + \mathcal{R}(z)\right]\mathcal{Z}_d - \mathcal{R}_d\tilde{\mathcal{Z}}\right) = 0. \tag{22}$$

By dismantling the matrices of (22), the following equations can be obtained

$$\begin{cases} \mu_1 E_1 - L_1\dot{z}_{1d} - z_{3d} + R_{1d}(z_1 - z_{1d}) = 0, \\ \mu_2 E_2 - L_2\dot{z}_{2d} - z_{3d} + R_{2d}(z_2 - z_{2d}) = 0, \\ -C_{eq}\dot{z}_{3d} + z_{1d} + z_{2d} - \dfrac{z_{3d}}{R} - \dfrac{P}{z_{3d}} + \dfrac{1}{R_{3d}}(z_3 - z_{3d}) = 0 \end{cases} \tag{23}$$

The energy shaping stage accomplished with the damping injection stage reinforce the energy of the entire system to be strictly passive (stable). For this reason the PBC strategy is able to regulate and damp the energy oscillation of the DC-bus voltage caused by the CPLs. Equation (23) provides the sufficient and necessary information to describe the dynamic characteristics of the PBC strategy. It can be seen, that three dynamic equations are available to solve, however four degrees of freedom should be determined (z_{1d}, z_{2d}, z_{3d}, and μ). The control goal of the dc-bus voltage can easily be handled when the transient dynamics of the state variables ($\dot{z}_{1d}, \dot{z}_{2d}, \dot{z}_{3d}$) are vanished. Therefore, the following condition must be satisfied

$$\underbrace{[\, z_{1d} \;\; z_{2d} \;\; z_{3d} \,]^T}_{\textit{Auxiliary states}} \overset{\textit{Converge to}}{\longrightarrow} \underbrace{[\, I_{L1} \quad I_{L2} \quad V_o \,]^T}_{\textit{Equilibrium points}}$$

Finally, (23) can be reformulated as follows

$$\mu_1 = \frac{1}{E_1}\left[V_o + R_{1d}\left(I_{L1} - i_{L1}\right)\right]. \tag{24}$$

$$\mu_2 = \frac{1}{E_2}\left[V_o + R_{2d}\left(I_{L2} - i_{L2}\right)\right]. \tag{25}$$

$$I_{L1} = I_{L2} = \frac{1}{2}\left[\frac{V_o}{R} + \frac{P}{V_o} + \frac{1}{R_{3d}}\left(V_o - v_o\right)\right]. \tag{26}$$

The control objective of the PBC strategy is obtained by (24), (25) and (26) as shown in Fig. 5. The equalization condition of the output current would be satisfied when references of the inductor currents are be equal ($I_{L1} = I_{L2}$). The control signals (μ_1, μ_2) are synthesized based on the inductor current feedback (the inner-loop control). Whereas the references of the inductor currents (I_{L1}, I_{L2}) are adjusted using the input of the outer-loop control (dc-bus voltage feedback). The PBC strategy can easily damps the oscillation caused by the CPL and regulates the dc-bus voltage properly. It can also ensures equal current sharing condition for the non-identical dc-dc power converters. Table 1 shows the non-identical parameters of the parallel dc-dc buck power converters with the loads. However, the main drawback of this control scheme is that it cannot eliminate the steady-state error caused by the system disturbances.

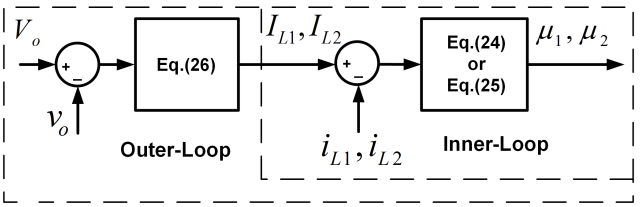

FIGURE 5. Duty ratios synthesizing of the PBC strategy based on the outer and inner loop control.

TABLE 1. System parameters.

Descriptions	Nominal Values
Inductances	$L_{1o} = 4\ mH,\ L_{2o} = 10\ mH$
Capacitances	$C_{1o} = 1000\ \mu F,\ C_{2o} = 470\ \mu F$
CPL power	$P_o = 14.44\ kW$
Load resistance	$R_o = 50\ \Omega$
Input Voltages	$E_{1o} = E_{2o} = 1500\ V$
Desired Dc-bus voltage	$V_o = 750\ V$

Fig. 6 shows the dc-bus voltage and indcutor currents waveforms of the dc-dc source power converters feeding the CPL and CVL. Initially the parallel converters are adjusted to operate in open-loop control (fixed duty ratio), then at $t = 0.1\ s$, the PBC is applied. Because every source-subsystem is complied by self-disciplined passivity, we can see that the oscillation dynamics is suppressed and the dc-bus

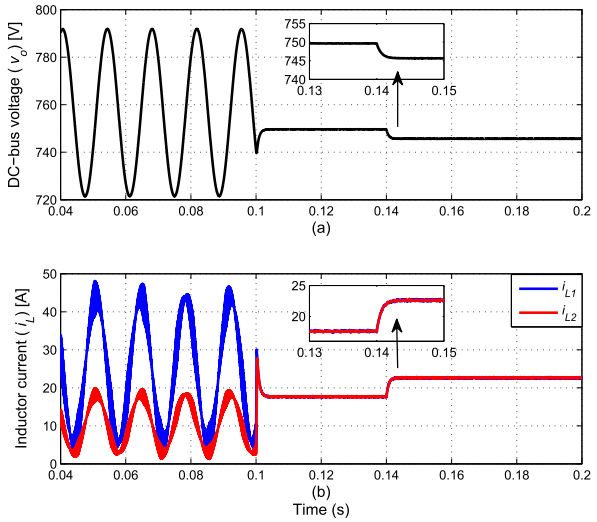

FIGURE 6. Dynamic response of the two parallel dc-dc buck power converters working at three different operating modes; open-loop control (fixed duty ratio), closed-loop control (PBC), and a sudden change in a CPL.

voltage is accurately controlled at 750 V. However, when the power of the CPL is changed from 14.44 to 21.66 kW at $t = 0.14$ s, the PBC strategy is failed to eliminate the steady-state error of the dc-bus voltage. This error is eliminated by adding integral term to (24) and (25), [29], [31]. However, it causes additional performance problems such as high overshoot dynamics and long settling time. In [34], [36], the NDO was applied not only to eliminate this error, but also to improve the control robustness of the PBC during system disturbances. However, it was only applied for a single dc-dc buck power converter feeding a CPL + CVL [36]. The following section introduces the NDO for the parallel dc-dc buck power converters feeding a CPL + CVL.

III. NONLINEAR DISTURBANCE OBSERVER DESIGN FOR THE PARALLEL-CONNECTED CONVERTERS

A. NONLINEAR DISTURBANCE OBSERVER

The majority of the above mentioned PBC strategies (PD-PBC, PBIC, and IDA-PBC) are used to reject the disturbances of the system using the feedback control system with integral gain rather than feedforward compensation control [29]–[32]. The disturbances rejection is generally take place via integral gain based on the tracking error between the desired value and the measured value. This may lead to attenuate the disturbances of the system in a relatively slow way. Thus, the previous PBC controllers cannot react fast enough at the wide load and input voltage variations. Therefore, the resulted regulation performance is slow with limited recovery performance [32], [34], [36]. In control systems, the feedforward compensation control is superiored because it provides an effective disturbance compensation tool that can achieve prompt disturbance attenuation. The input states to the feedforward control can be obtained by direct measurements, or it can be estimated using nonlinear disturbance observer (NDO). The NDO can reject the disturbance of the system online with less information dynamics and operates in parallel with the PBC strategy to estimate and compensate the disturbances of the system through a feedforward compensation channel. The estimated values of the disturbances $\hat{d} = \left[\hat{d}_1\ \hat{d}_2\ \hat{d}_3\right]^T$ can be added to the PBC equations (24), (25) and (26) to compensate the amount of the steady-state error as follows:

$$\begin{cases} \mu_1 = \dfrac{1}{E_1}\left[V_o + R_{1d}\left(I_{L1} - i_{L1}\right) - \hat{d}_1\right], \\ \mu_2 = \dfrac{1}{E_2}\left[V_o + R_{2d}\left(I_{L2} - i_{L2}\right) - \hat{d}_2\right], \\ I_{L1} = I_{L2} = \dfrac{1}{2}\left[\dfrac{V_o}{R} + \dfrac{P}{V_o} + \dfrac{1}{R_{3d}}\left(V_o - v_o\right) - \hat{d}_3\right]. \end{cases} \tag{27}$$

Equation (3) is a class of affine nonlinear equations, which satisfies the following matrix form according to [38], [39].

$$\begin{cases} \dot{z} = f(z) + g_1(z)\mu + g_2(z)d, \\ y_o = h(z), \end{cases} \tag{28}$$

where

$$\dot{z} = \begin{pmatrix} \dot{z}_1 \\ \dot{z}_2 \\ \dot{z}_3 \end{pmatrix}, \quad f(z) = \begin{pmatrix} -\dfrac{z_3}{L_1} \\ -\dfrac{z_3}{L_2} \\ \dfrac{z_1}{C_{eq}} + \dfrac{z_2}{C_{eq}} - \dfrac{z_3}{C_{eq}R} - \dfrac{P}{C_{eq}z_3} \end{pmatrix}$$

$$g_1(z) = \begin{pmatrix} \dfrac{E_1}{L_1} \\ \dfrac{E_2}{L_2} \\ 0 \end{pmatrix}, \quad g_2(z) = \begin{pmatrix} 1 & 0 & 0 \\ 0 & 1 & 0 \\ 0 & 0 & 1 \end{pmatrix},$$

y_o is the output vector of the system and $h(z)$ is the smooth function matrix in terms of z. The disturbances in dc microgrids are a type of constant disturbances that have unknown values, which can be estimated using the following basic nonlinear disturbance observer [38], [39].

$$\dot{\hat{d}} = \ell\left(z\right)\left[\dot{z} - f\left(z\right) - g_1\left(z\right)\mu - g_2(z)\hat{d}\right] \tag{29}$$

where $\ell(z) = (dp(z)/dz)$ represents the nonlinear gain of the observer and the $p(z)$ is the nonlinear function to be designed. The desired estimated magnitudes of the unknown disturbances can be obtained by the following dynamic equations [36], [38], [40].

$$\begin{cases} \dot{y} = -\ell(z)g_2(z)y - \ell(z)\left[g_2(z)p(z) + f(z) + g_1(z)\mu\right] \\ \hat{d} = y + p(z). \end{cases} \tag{30}$$

where $y \in \mathbb{R}^l$ is the internal state vector of the nonlinear observer. The stability condition of the NDO can be ensured when estimated disturbances $\hat{d}$ converge to the real disturbances d of the system. Defining the disturbance error

$$e_r = \hat{d} - d \tag{31}$$

The transient dynamic of the error can be written as

$$\dot{e}_r = \dot{\hat{d}} - \dot{d} \tag{32}$$

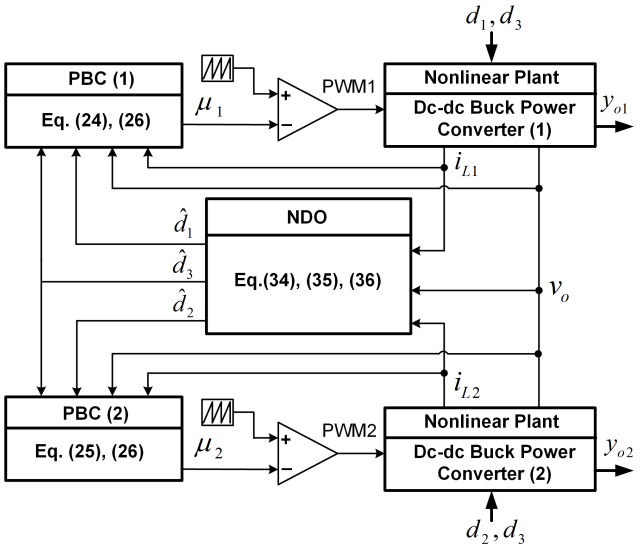

FIGURE 7. Block diagram representing the composite control strategy (PBC with NDO) and the nonlinear plant.

By invoking (28) and (29) into (32), the error dynamic can be written as

$$\dot{e}_r = -\ell(z)g_2(z)e_r \tag{33}$$

According to the Lyapunov sense, the dynamic error in (33) is asymptotically approach to zero pending on the the values of observer gain $\ell(z)$

$$\ell(z) = \begin{pmatrix} \lambda_1 & 0 & 0 \\ 0 & \lambda_2 & 0 \\ 0 & 0 & \lambda_3 \end{pmatrix} \quad \text{and thus } p(z) = \begin{pmatrix} \lambda_1 i_{L1} \\ \lambda_2 i_{L2} \\ \lambda_3 v_o \end{pmatrix}.$$

Finally, the dynamic equations of the estimated disturbances ($\hat{d}_1$, $\hat{d}_2$ and $\hat{d}_3$) can be achieved by substituting the values of $f(z)$, $\ell(z)$, $g_1(z)$, $g_2(z)$ and $p(z)$ in (30), which yields

$$\begin{cases} \dot{y}_1 = -\lambda_1 y_1 + \lambda_1 \left[-\dfrac{E_{1o}}{L_{1o}}\mu_1 + \dfrac{v_o}{L_{1o}} - \lambda_1 i_{L1} \right] \\ \hat{d}_1 = y_1 + \lambda_1 i_{L1}. \end{cases} \tag{34}$$

$$\begin{cases} \dot{y}_2 = -\lambda_2 y_2 + \lambda_2 \left[-\dfrac{E_{2o}}{L_{2o}}\mu_2 + \dfrac{v_o}{L_{2o}} - \lambda_2 i_{L2} \right] \\ \hat{d}_2 = y_2 + \lambda_2 i_{L2}. \end{cases} \tag{35}$$

$$\begin{cases} \dot{y}_3 = -\lambda_3 y_3 + \lambda_3 \left[-\dfrac{i_L}{C_{eqo}} + \dfrac{v_o}{C_{eqo}R_o} + \dfrac{P_o}{C_{eqo}v_o} - \lambda_3 v_o \right] \\ \hat{d}_3 = y_3 + \lambda_3 v_o. \end{cases} \tag{36}$$

where $i_L = i_{L1} + i_{L2}$. Equations (34), (35) and (36) are fully describe the dynamic behavior of the NDO. Using these equations, the real disturbance (uncertainty) of the system can be estimated and fed into the PBC closed-loop equation (27). Fig. 7 shows a typical block diagram of the composite nonlinear plant (dc-dc buck power converters with CPL & CVL) and the nonlinear control scheme (PBC with NDO).

B. PASSIVITY-BASED I-V DROOP CONTROL

The unequal current sharing or circulating current problem in DC microgrids is occurring due to the voltage mismatch between the output of the parallel source converters. In [44], it was proved that 1% mismatch between output voltages is enough to lose the equal current sharing property and circulate the currents between converters terminals. In the design of the passivity-based controller (26), the reference currents I_{L1}, I_{L2} are controlled based on the measurement of the dc-bus voltage v_o, which concurs with *I-V* droop control [47]. Previously in (26), we assume that the reference of dc-bus voltage and the reference voltage of the parallel converters are equal $V_o = V_{o1} = V_{o2}$; if not, Equation (26) can be rewritten as

$$\begin{cases} I_{L1} = \dfrac{1}{2}\left[\dfrac{V_{o1}}{R} + \dfrac{P}{V_{o1}} + \dfrac{1}{R_{3d}}(V_{1o} - v_o) \right], \\ I_{L2} = \dfrac{1}{2}\left[\dfrac{V_{o2}}{R} + \dfrac{P}{V_{o2}} + \dfrac{1}{R_{3d}}(V_{2o} - v_o) \right]. \end{cases} \tag{37}$$

The *I-V* droop control able to eliminate the deviation in the dc-bus voltage caused by the voltage mismatch between the parallel converters as well as getting equal current sharing [46], [47].

$$I_{Ld1} = \frac{1}{R_1}(V_{o1} - v_o), \quad I_{Ld2} = \frac{1}{R_2}(V_{o2} - v_o). \tag{38}$$

where I_{Ld1}, I_{Ld2} are the reference currents derived from the *I-V* droop characteristics. Fig. 8 depicts the *I-V* linear droop characteristics to control the reference current I_{L1}, I_{L2} according to the droop curve and measurement of the dc-bus voltage. The currents derived by the droop control I_{Ld1}, I_{Ld2} are injected to the PBC strategy (37) to compensate the amplitude of voltage mismatch between the parallel converters.

$$\begin{cases} I_{L1new} = \dfrac{1}{2}\left[\dfrac{V_{o1}}{R} + \dfrac{P}{V_{o1}} + \dfrac{1}{(R_{3d} + R_1)}(V_{1o} - v_o) \right], \\ I_{L2new} = \dfrac{1}{2}\left[\dfrac{V_{o2}}{R} + \dfrac{P}{V_{o2}} + \dfrac{1}{(R_{3d} + R_2)}(V_{2o} - v_o) \right]. \end{cases} \tag{39}$$

The design of the PBC including *I-V* droop control should consider the trade-off between fast response dynamic and accurate current sharing. As future trend, the droop gains (R_1, R_2) can be variable values to be adaptive according to the magnitude of voltage mismatch between the converters.

IV. MATLAB SIMULATION AND HARDWARE-IN-LOOP EXPERIMENTAL RESULTS

In this section the MATLAB simulation results of the proposed controller (PBC with NDO) have been verified using HIL experiment platform. The HIL is implemented via real hardware digital signal processor (DSP) and real time simulator. Fig. 9 depicts the laboratories construction of HIL simulation platform including the MATLAB simulation system connected to the hardware DSP (TMS320F28035) through the real-time simulator (OPAL-RT OP5600). The signal received from OPAL-RT analog/output is converted to digital signals through analog/digital converter (ADC).

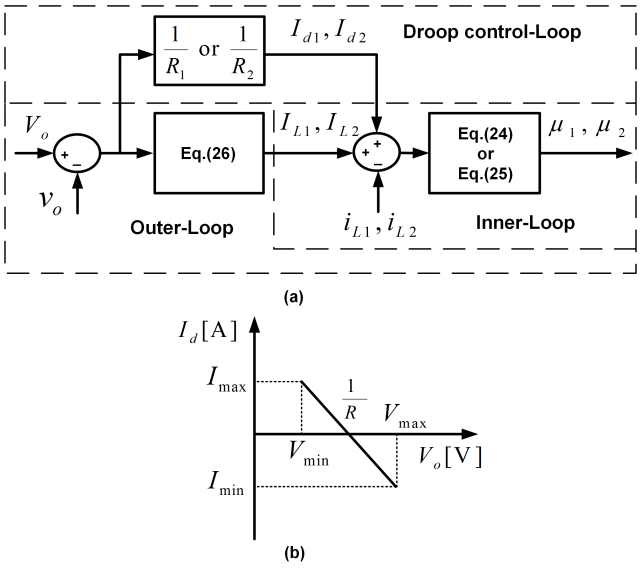

FIGURE 8. (a) Duty ratios synthesizing for the PBC strategy based on the inner-loop, outer-loop, and droop-loop control, (b) *I-V* droop control characteristics.

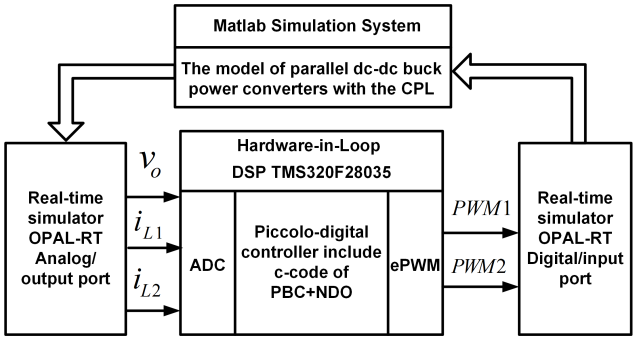

FIGURE 9. The HIL platform contains the MATLAB simulated model (parallel dc-dc buck power converters) connected to the TMS320F28035 C2000 microcontroller thorough the OPAL-RT real-time simulator.

The C-code is generated via MATLAB Simulink generation code with code composer studio software based on the digital input signals v_o, i_{L1} and i_{L2}. The code outputs are the duty cycles of parallel converters, which in turn become the inputs for the enhanced pulsewidth modulator modules (PWM1 & PWM2). The signals are then fed back to the MATLAB simulation system. The control gains of the closed-loop systems are selected as; (a) The PBC gains $R_{1d} = R_{2d} = 1 \times 10^6$ and $R_{3d} = 0.4$, (b) The NDO gains $\lambda_1 = 100$, $\lambda_2 = 40$ and $\lambda_3 = 1470$. The PBC and the NDO gains have been adjusted to ensure energy dissipation to the limit-cycle dynamics and to guarantee the trajectory convergence to the desired equilibrium points. The idea behind the values selection of the PBC gains (R_{1d}, R_{2d}, R_{3d}) is that, the sufficiently large values of virtual series resistances (R_{1d}, R_{2d}) with the inductor circuits ensure high energy dissipation and better ripples suppression for the inductor currents. Whereas, the small value of the parallel virtual resistance (R_{3d}) with the capacitor circuits guarantee the energy dissipation across the capacitor circuits and lead to damp the ripples of the output voltage. Similarly, the value of the NDO gains (λ_1, λ_2 and λ_3) are selected to ensure the estimated disturbances of the system are precisely converging to the real disturbances. To this end, the tuning of the NDO gains should consider the trade-off between the convergence condition and fast response to the system disturbances.

A. ROBUSTNESS VERIFICATION OF THE PROPOSED CONTROL STRATEGY

To verify the robustness of the proposed controller, the MATLAB simulation and HIL experimental results are carried out for four types of disturbances.

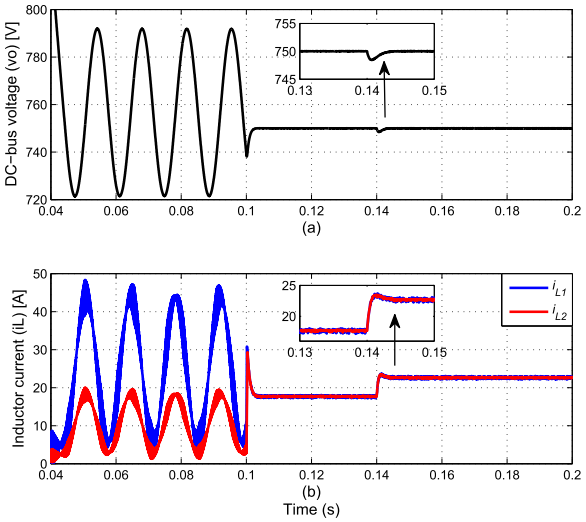

FIGURE 10. Dynamic response of the two parallel dc-dc buck power converters working at three different operating modes; open-loop control (fixed duty ratio), closed-loop control (PBC + NDO), and a sudden change in a CPL.

1) SYSTEM BEHAVIOR DURING CPL DISTURBANCE

In this section, the NDO is added to work in parallel with the PBC closed-loop system. Similar to Fig. 6, Fig. 10 shows the dynamic waveforms of the dc-bus voltage and the inductor currents. Because of the different circuit parameters, the waveforms exhibits different limit cycle dynamics at open-loop control. The proposed controller (PBC with NDO) is then applied at $t = 0.1$ s, we can see that the dc-bus voltage is accurately controlled at 750 V. At time $t = 0.14$ s, the CPL is changed from 14.44 to 21.66 kW. At this time, the NDO is triggered, and therefore, the steady-state error is eliminated with extremely fast recovery performance. Fig. 11 shows the simulation results by means of real time simulator and HIL experiment to verify the MATLAB results obtained in Fig. 10. In OPAL-RT OP5600, the maximum and minimum voltage operating limits are ±16 V. Because of this limitation, the dc-bus voltage v_o is scaled down. Therefore, the reference voltage line at the scope is adopted at 720 V. Therefore, the sum of the scope reading 30 V plus reference voltage 720 V resulted 750 V.

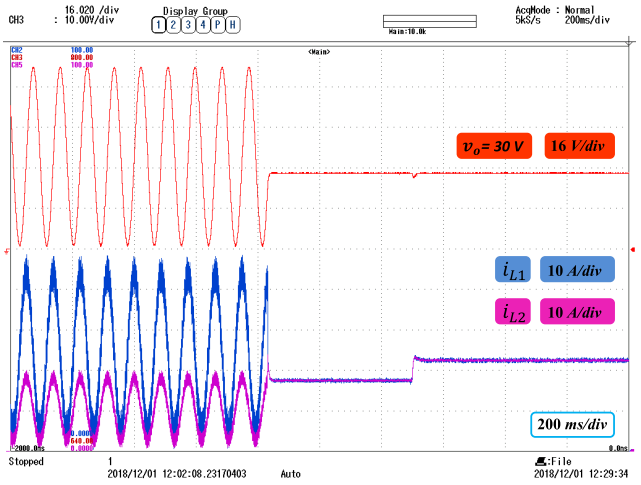

FIGURE 11. HIL real time dynamics to validate the MATLAB simulation results obtained in Fig. 10.

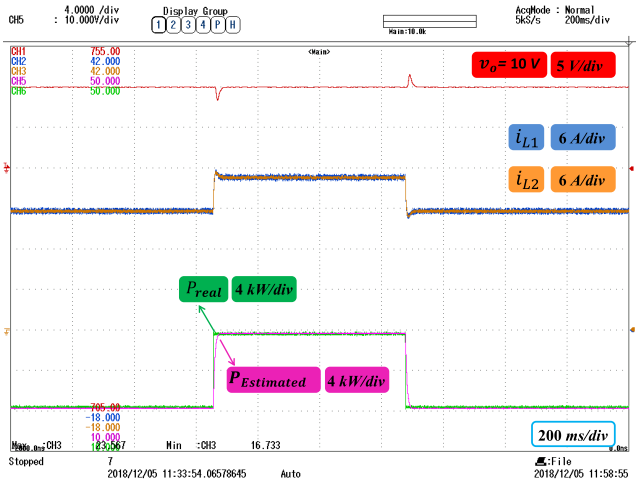

FIGURE 13. Dynamic response traces using HIL real time simulator to verify the MATLAB simulation results depicted in Fig. 12.

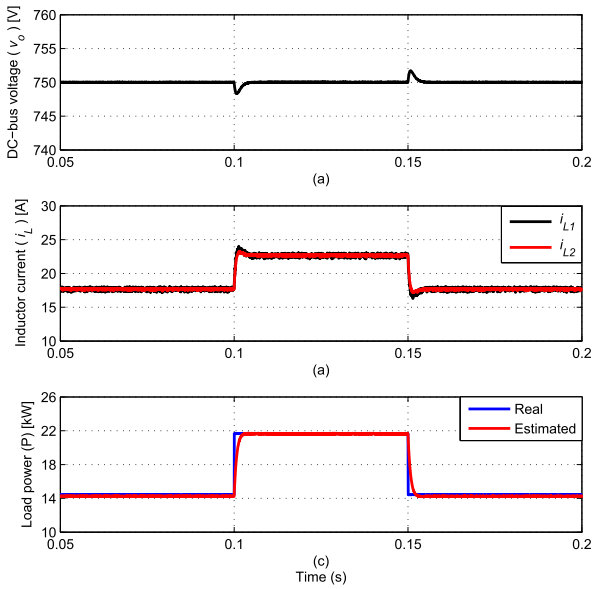

FIGURE 12. Dynamic performance of (a) the dc-bus voltage, (b) inductor currents waveforms of the two parallel dc-dc buck power converters subjected to a CPL changes, and (c) the real and estimated power using the NDO.

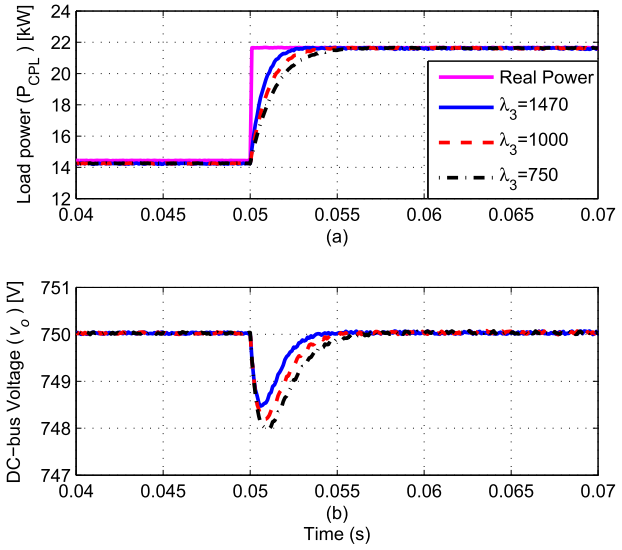

FIGURE 14. Dynamic response of the (a) real and estimated power of the CPL, (b) dc-bus voltage during CPL changes with different values of the control gain λ_3.

The effectiveness of the NDO has also verified during the CPL changes (see Fig. 12). It can be seen that, the proposed control strategy provide a robust voltage control against CPL variation and fast convergence performance between the estimated and real power of the CPL (within millisecond range). Fig. 13 depicts the HIL experimental results to verify the performance of the MATLAB simulation results demonstrated in Fig. 12. We can observe that, the proposed controller provides a robust control dynamic against the CPL changes and the convergence of estimated power to the real power is relatively accurate. In this case, the reference line of scope for the dc-bus voltage trace is adjusted at 740 V. Therefore, the sum of the scope reading 10 V plus 740 V is equal 750 V.

Further verifications were also implemented to investigate the control performance at different control gains. Fig. 14 shows the effect of the NDO gain λ_3 on control performance. It can be seen that, the convergence of the estimated power to the real power is improved by increasing the control gain λ_3. Therefore, the control robustness of the dc-bus voltage v_o is also improved (see Fig. 14(b)). This implies that, the NDO not only able to eliminate the steady-state error but also can increase the degree of control freedom. The control performance of the adaptive PBC strategy is also verified at different control gains of R_{3d} as shown in Fig. 15. We can notice that, the decreases of R_{3d} lead to a fast recovery performance. We can conclude that, the robust control dynamic and fast recovery performance can be achieved as long as the value of λ_3 increases and the value of the R_{3d} decreases.

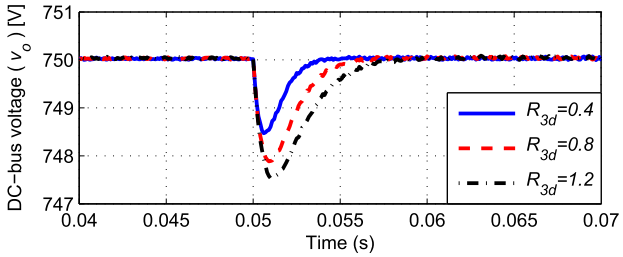

FIGURE 15. Dynamic response of the dc-bus voltage during CPL changes with different values of the control gain R_{3d}.

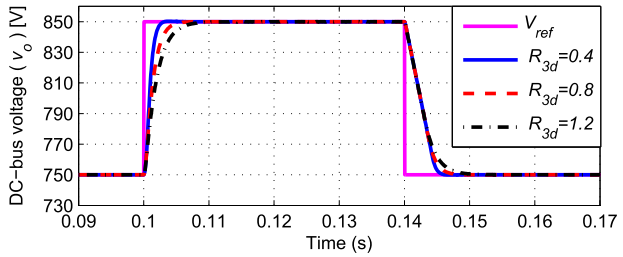

FIGURE 16. Tracking performance of the dc-bus voltage to the reference voltage with different values of the control gain R_{3d}.

2) SYSTEM BEHAVIOR DURING REFERENCE VOLTAGE DISTURBANCE

Fig. 16 shows the dynamic behavior of the dc-bus voltage tracking to the changes of the reference voltage V_{ref}. Initially, the reference voltage is fixed at 750 V. At time $t = 0.1\ s$ the reference voltage is changed up to 850 V then is returned down to 750 V. Various values of the control gain R_{3d} have been applied to clarify the tracking performance of the proposed controller. It can be seen that, the dc-bus voltage is precisely converged to the reference voltage with fast dynamic performance. Similar dynamic performance is achieved using the HIL simulation platform (see Fig. 17). In this case, the reference line voltage of scope is taken at 740 V. Within a millisecond range the proposed controller provides fast tracking response to the different set points.

3) SYSTEM BEHAVIOR DURING LINE DISTURBANCE

In this section, the control performance of the PBC with NDO has been verified during line disturbances (i.e. input voltage changes). Fig. 18 depicts the dynamic behavior of the dc-bus voltage and the inductor current during input voltages changes (E_1, E_2). Initially, the input voltages of both converters are fixed at 1500 V. At $t = 0.1\ s$, the input voltage E_1 is increased up to 1750 V, while the input voltage E_2 is increased up to 2000 V. It can be seen that, the regulating performance of the dc-bus voltage not affected by the large variations of the input voltages. The HIL real time simulation results of Fig. 18 have been depicted in Fig. 19.

4) FEEDBACK PBC WITH INTEGRAL VERSUS FEEDFORWARD BASED PBC WITH NDO

Fig. 20 and Fig. 21 show a fair comparison between the PBC strategy [26], PBC strategy with the integral (PBC + I) [7], and the proposed PBC strategy with NDO (PBC + NDO).

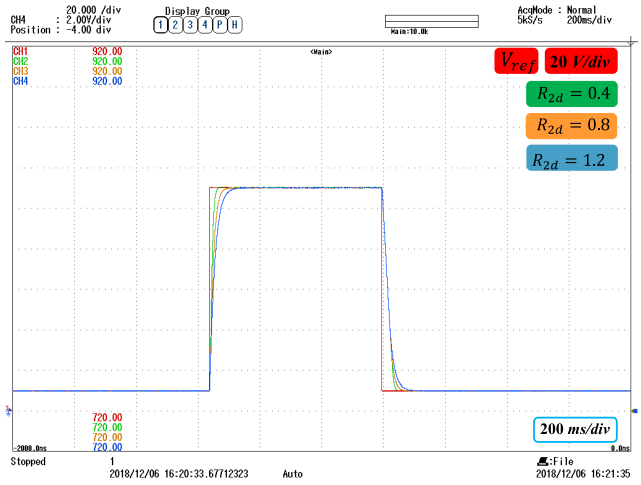

FIGURE 17. HIL real time dynamics to validate the MATLAB simulation results obtained in Fig. 16.

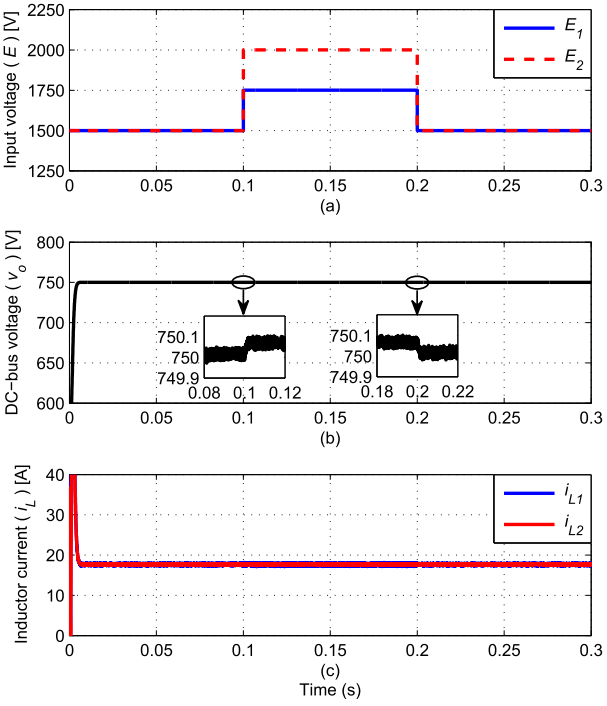

FIGURE 18. Dynamic performance of the dc-bus voltage and the inductor currents during input voltage changes.

At startup, the dc-bus voltage is controlled at 750 V and the CPL is loaded by 14.44 kW, then the CPL is suddenly increased up to 21.66 kW (see Fig. 20) and decreased down to 7.22 kW (see Fig. 21), respectively. The results show the superiority of the feedforward control system based the PBC + NDO over the conventional feedback control combined with the integral gain PBC + I. The PBC strategy with the NDO attenuates the disturbances (due to CPL changes) extremely fast with shortest settling time as compared with the PBC strategy plus integral. Based on a feedforward compensation control, the PBC + NDO strategy provide a very

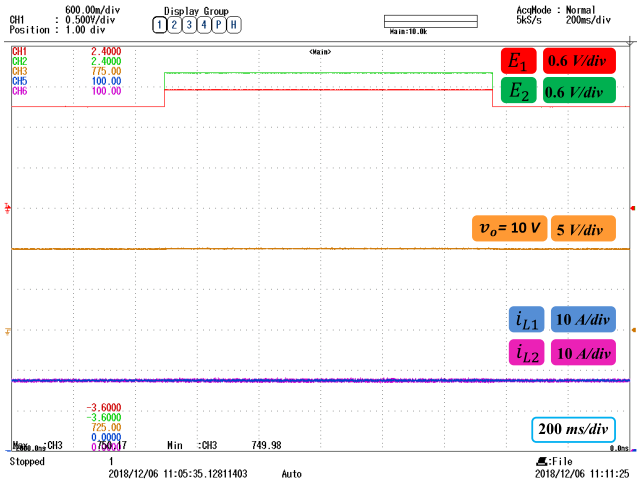

FIGURE 19. HIL real time dynamic results to validate the results obtained in Fig. 18.

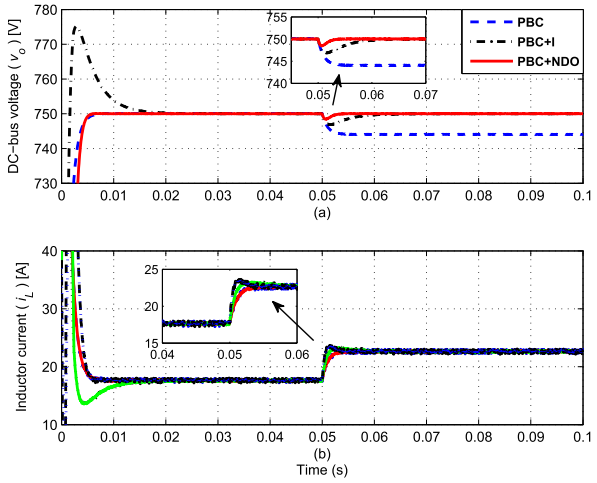

FIGURE 20. Dynamic behavior of the parallel dc-dc buck power converters subjected to a sudden change in CPL from 14.44 *kW* to 21.66 *kW* at $t = 0.05$ *s*.

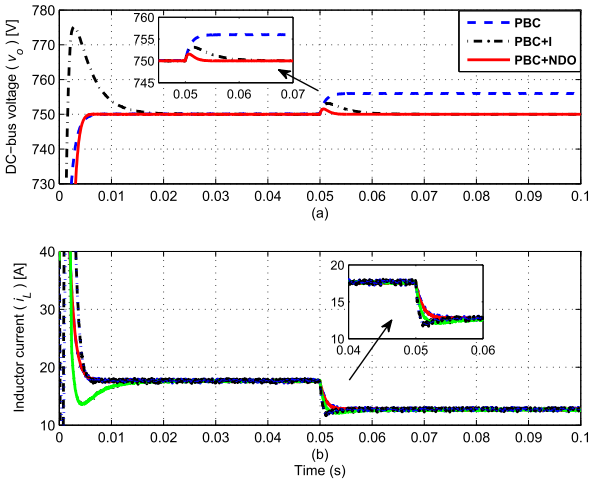

FIGURE 21. Dynamic behavior of the parallel dc-dc buck power converters subjected to a sudden change in CPL from 14.44 *kW* to 7.22 *kW* at $t = 0.05$ *s*.

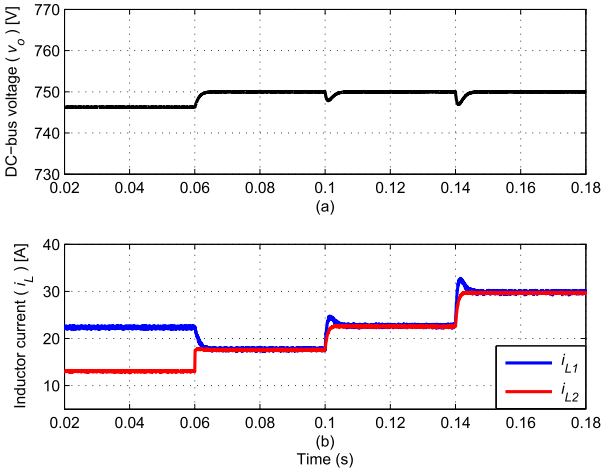

FIGURE 22. Dynamic performance of the two parallel dc-dc buck power converters working at three different operating modes; voltage mismatch, CPL variation from 14 kW to 21.66 kW, and CPL variation from 21.66 to 32 kW.

short settling time at startup of operation as compared with the PBC + I, which depicts an exceptional high overshoot due the integral gain.

B. SYSTEM BEHAVIOR DURING MISMATCH BETWEEN THE CONVERTERS OUTPUT VOLTAGES

The dynamic of the NDO is only able to estimate the disturbances in the output voltage caused by the load and line variation; the voltage mismatch between the parallel converters cannot be handled. Based on the self *I-V* droop property of the PBC strategy, this problem can be solved by adding more virtual resistance to reshape the energy flow across the capacitor circuit, thereby eliminating the output voltage mismatch by getting equal current sharing. Fig. 22 shows the dynamic waveforms of the dc-bus voltage and the inductor currents. Initially the system works with 1% voltage mismatch between the parallel converters; therefore, Fig. 22 shows unequal current sharing. The *I-V* droop control is then applied at $t = 0.06$ *s* through adding a large virtual resistance ($R_2 = 50$). This resistance is added to eliminate the voltage difference between parallel converters. At time $t = 0.1$ *s* and $t = 0.14$ *s*, the CPL changed from 14 to 21.66 kW and to 32 kW respectively. It can observe that, the condition of the equal current sharing is precisely obtained at large variations on the CPL, as well as the dc-bus voltage is properly regulated at 750 V. To consider the trade-off between fast response dynamic and accurate current sharing, the droop gains (R_1, R_2) should be varied according to the magnitude of the voltage mismatch between the parallel converters, which can be considered as the future trends for this work.

V. CONCLUSION

This paper addresses the instability problem caused by the CPLs for the parallel-contented dc-dc buck power converters

in dc microgrid systems. To solve this problem, the adaptive PBC strategy with NDO is applied to stabilize the oscillation caused by the CPLs as well as to compensate the disturbances of the dc microgrid system. The NDO is applied to eliminate the steady-state error of PBC caused by the system disturbances as well as to increase the degree of control freedom. This controller provides superior anti-disturbance rejection with extremely recovery performance as compared with other PBC strategies. Based on the passivity property, the concept of the *I-V* droop control is also emphasized to ensure both voltage regulation and equal current sharing. The MATLAB simulation and HIL experiment results are presented to verify the control performance of the proposed controller.

REFERENCES

[1] L. E. Zubieta, "Are microgrids the future of energy?: DC microgrids from concept to demonstration to deployment," *IEEE Electrific. Mag.*, vol. 4, no. 2, pp. 37–44, Jun. 2016.

[2] T. Dragicevic, X. Lu, J. C. Vasquez, and J. M. Guerrero, "DC Microgrids—Part I: A review of control strategies and stabilization techniques," *IEEE Trans. Power Electron.*, vol. 31, no. 7, pp. 4876–4891, Jul. 2016.

[3] J. M. Guerrero and D. F. D. Tan, "Guest editorial special issue on structured DC microgrids," *IEEE J. Emerg. Sel. Topics Power Electron.*, vol. 5, no. 3, pp. 925–927, Sep. 2017.

[4] P. F. Donoso Garcia, P. C. Cortizo, B. R. de Menezes, and M. A. Severo Mendes, "Sliding mode control for current distribution in DC-to-DC converters connected in parallel," in *Proc. Rec. 27th Annu. IEEE Power Electron. Specialists Conf. (PESC)*, vol. 2, Jun. 1996, pp. 1513–1518.

[5] A. Emadi, A. Khaligh, C. H. Rivetta, and G. A. Williamson, "Constant power loads and negative impedance instability in automotive systems: Definition, modeling, stability, and control of power electronic converters and motor drives," *IEEE Trans. Veh. Technol.*, vol. 55, no. 4, pp. 1112–1125, Jul. 2006.

[6] S. Singh, A. R. Gautam, and D. Fulwani, "Constant power loads and their effects in DC distributed power systems: A review," *Renew. Sustain. Energy Rev.*, vol. 72, pp. 407–421, May 2017.

[7] A. Kwasinski and P. T. Krein, "Passivity-based control of buck converters with constant-power loads," in *Proc. IEEE Annu. Power Electron. Specialists Conf. (PESC)*, Jun. 2007, pp. 259–265

[8] A. Riccobono and E. Santi, "Comprehensive review of stability criteria for DC power distribution systems," *IEEE Trans. Ind. Appl.*, vol. 50, no. 5, pp. 3525–3535, Sep. 2014.

[9] R. D. Middlebrook, "Input filter considerations in design and application of switching regulators," in *Proc. IEEE Ind. Appl. Soc. Annu. Meeting*, Oct. 1976, pp. 366–382.

[10] X. Feng, J. Liu, and F. C. Lee, "Impedance specifications for stable DC distributed power systems," *IEEE Trans. Power Electron.*, vol. 17, no. 2, pp. 157–162, Mar. 2002.

[11] X. Wang, R. Yao, and F. Rao, "Three-step impedance criterion for small-signal stability analysis in two-stage DC distributed power systems," *IEEE Power Electron Lett.*, vol. 1, no. 3, pp. 83–87, Sep. 2003.

[12] A. Riccobono and E. Santi, "Positive feedforward control of three-phase voltage source inverter for DC input bus stabilization with experimental validation," *IEEE Trans. Ind. Appl.*, vol. 49, no. 1, pp. 168–177, Jan. 2013.

[13] M. Cespedes, L. Xing, and J. Sun, "Constant-power load system stabilization by passive damping," *IEEE Trans. Power Electron.*, vol. 26, no. 7, pp. 1832–1836, Jul. 2011.

[14] R. W. Erickson and D. Maksimvíc, *Fundamentals of Power Electronics*, 2nd ed. New York, NY, USA: Kluwer, 2011, ch. 10.

[15] M. Wu and D. D.-C. Lu, "Active stabilization methods of electric power systems with constant power loads: A review," *J. Mod. Power Syst. Clean Energy*, vol. 2, no. 3, pp. 233–243, Sep. 2014.

[16] X. Chang, Y. Li, X. Li, and X. Chen, "An active damping method based on a supercapacitor energy storage system to overcome the destabilizing effect of instantaneous constant power loads in DC microgrids," *IEEE Trans. Energy Convers.*, vol. 32, no. 1, pp. 36–47, Mar. 2017.

[17] H. Chen and N. Sun, "Nonlinear control of underactuated systems subject to both actuated and unactuated state constraints with experimental verification," *IEEE Trans. Ind. Electron.*, vol. 67, no. 9, pp. 7702–7714, Sep. 2020.

[18] M. Su, Z. Liu, Y. Sun, H. Han, and X. Hou, "Stability analysis and stabilization methods of DC microgrid with multiple parallel-connected DC–DC converters loaded by CPLs," *IEEE Trans. Smart Grid*, vol. 9, no. 1, pp. 132–142, Jan. 2018.

[19] D. K. Fulwani and S. Singh, *Mitigation of Negative Impedance Instabilities in DC Distribution Systems*. Singapore: Springer, 2017.

[20] T. Dragicevic, "Dynamic stabilization of DC microgrids with predictive control of Point-of-Load converters," *IEEE Trans. Power Electron.*, vol. 33, no. 12, pp. 10872–10884, Dec. 2018.

[21] Q. Xu, C. Zhang, C. Wen, and P. Wang, "A novel composite nonlinear controller for stabilization of constant power load in DC microgrid," *IEEE Trans. Smart Grid*, vol. 10, no. 1, pp. 752–761, Jan. 2019.

[22] S. Yousefizadeh, J. D. Bendtsen, N. Vafamand, M. H. Khooban, F. Blaabjerg, and T. Dragicevic, "Tracking control for a DC microgrid feeding uncertain loads in more electric aircraft: Adaptive backstepping approach," *IEEE Trans. Ind. Electron.*, vol. 66, no. 7, pp. 5644–5652, Jul. 2019.

[23] I. Kondratiev, E. Santi, R. Dougal, and G. Veselov, "Synergetic control for DC-DC buck converters with constant power load," in *Proc. IEEE 35th Annu. Power Electron. Specialists Conf.*, vol. 5, Jun. 2004, pp. 3758–3764.

[24] Y. Gu, W. Li, and X. He, "Passivity-based control of DC microgrid for self-disciplined stabilization," *IEEE Trans. Power Syst.*, vol. 30, no. 5, pp. 2623–2632, Sep. 2015.

[25] J. C. Willems, "Dissipative dynamical systems part I: General theory," *Arch. for Rational Mech. Anal.*, vol. 45, no. 5, pp. 321–351, 1972.

[26] R. Ortega, A. Loría, P. J. Nicklasson, and H. Sira-Ramírez, *Passivity-Based Control of Euler-Lagrange Systems* (Communications and Control Engineering). London, U.K.: Springer, 1998.

[27] H. Sira-Ramírez, R. Ortega, and M. García-Esteban, "Adaptive passivity-based control of average DC-to-DC power converter models," *Int. J. Adapt. Control Signal Process.*, vol. 12, no. 1, pp. 63–80, Feb. 1998.

[28] A. Kwasinski and C. N. Onwuchekwa, "Dynamic behavior and stabilization of DC microgrids with instantaneous constant-power loads," *IEEE Trans. Power Electron.*, vol. 26, no. 3, pp. 822–834, Mar. 2011.

[29] Y. I. Son and I. H. Kim, "Complementary PID controller to passivity-based nonlinear control of boost converters with inductor resistance," *IEEE Trans. Control Syst. Technol.*, vol. 20, no. 3, pp. 826–834, May 2012.

[30] R. Leyva, I. Queinnec, L. Martinez-Salamero, C. Alonso, A. Cid-Pastor, and S. Tarbouriech, "Passivity-based integral control of a boost converter for large-signal stability," *IEE Proc. Control Theory Appl.*, vol. 153, no. 2, pp. 139–146, Mar. 2006.

[31] J. Zeng, Z. Zhang, and W. Qiao, "An interconnection and damping assignment passivity-based controller for a DC-DC boost converter with a constant power load," *IEEE Trans. Ind. Appl.*, vol. 50, no. 4, pp. 2314–2322, Jul./Aug. 2014.

[32] W. He, S. Li, J. Yang, and Z. Wang, "Incremental passivity based control for DC-DC boost converter with circuit parameter perturbations using nonlinear disturbance observer," in *Proc. 42nd Annu. Conf. IEEE Ind. Electron. Soc. (IECON)*, Oct. 2016, pp. 1353–1358.

[33] H. Chen, B. Xuan, P. Yang, and H. Chen, "A new overhead crane emergency braking method with theoretical analysis and experimental verification," *Nonlinear Dyn.*, vol. 98, no. 3, pp. 2211–2225, Nov. 2019.

[34] M. A. Hassan, T. Li, C. Duan, S. Chi, and E. P. Li, "Stabilization of DC-DC buck power converter feeding a mixed load using passivity-based control with nonlinear disturbance observer," in *Proc. IEEE Conf. Energy Internet Energy Syst. Integr. (EI2)*, Nov. 2017, pp. 1–6.

[35] M. Srinivasan and A. Kwasinski, "Autonomous hierarchical control of DC microgrids with constant-power loads," in *Proc. IEEE Appl. Power Electron. Conf. Exposit. (APEC)*, Mar. 2015, pp. 2808–2815.

[36] M. A. Hassan, E.-P. Li, X. Li, T. Li, C. Duan, and S. Chi, "Adaptive passivity-based control of DC–DC buck power converter with constant power load in DC microgrid systems," *IEEE J. Emerg. Sel. Topics Power Electron.*, vol. 7, no. 3, pp. 2029–2040, Sep. 2019.

[37] W.-H. Chen, D. J. Ballance, P. J. Gawthrop, and J. O'Reilly, "A nonlinear disturbance observer for robotic manipulators," *IEEE Trans. Ind. Electron.*, vol. 47, no. 4, pp. 932–938, Aug. 2000.

[38] W.-H. Chen, "Disturbance observer based control for nonlinear systems," *IEEE/ASME Trans. Mechatronics*, vol. 9, no. 4, pp. 706–710, Dec. 2004.

[39] S. Li, J. Yang, W. H. Chen, and X. Chen, *Disturbance Observer-Based Control, Methods and Applications*. Boca Raton, FL, USA: CRC Press, 2014.
[40] W. H. Chen, J. Yang, L. Guo, and S. Li, "Disturbance-observer-based control and related methods—An overview," *IEEE Trans. Ind. Electron.*, vol. 63, no. 2, pp. 1083–1095, Feb. 2016.
[41] L. Shengquan, L. Juan, T. Yongwei, S. Yanqiu, and C. Wei, "Model-based model predictive control for a direct-driven permanent magnet synchronous generator with internal and external disturbances," *Trans. Inst. Meas. Control*, vol. 42, no. 3, pp. 586–597, Feb. 2020.
[42] S. Li, M. Cao, J. Li, J. Cao, and Z. Lin, "Sensorless-based active disturbance rejection control for a wind energy conversion system with permanent magnet synchronous generator," *IEEE Access*, vol. 7, pp. 122663–122674, 2019.
[43] J. M. Guerrero, J. C. Vasquez, J. Matas, L. G. de Vicuna, and M. Castilla, "Hierarchical control of droop-controlled AC and DC microgrids—A general approach toward standardization," *IEEE Trans. Ind. Electron.*, vol. 58, no. 1, pp. 158–172, Jan. 2011.
[44] S. Augustine, M. K. Mishra, and N. Lakshminarasamma, "Adaptive droop control strategy for load sharing and circulating current minimization in low-voltage standalone DC microgrid," *IEEE Trans. Sustain. Energy*, vol. 6, no. 1, pp. 132–141, Jan. 2015.
[45] A. P. N. Tahim, D. J. Pagano, E. Lenz, and V. Stramosk, "Modeling and stability analysis of islanded DC microgrids under droop control," *IEEE Trans. Power Electron.*, vol. 30, no. 8, pp. 4597–4607, Aug. 2015.
[46] F. Gao, S. Bozhko, A. Costabeber, C. Patel, P. Wheeler, C. I. Hill, and G. Asher, "Comparative stability analysis of droop control approaches in Voltage-Source-Converter-Based DC microgrids," *IEEE Trans. Power Electron.*, vol. 32, no. 3, pp. 2395–2415, Mar. 2017.
[47] H. Wang, M. Han, R. Han, J. M. Guerrero, and J. C. Vasquez, "A decentralized current-sharing controller endows fast transient response to parallel DC–DC converters," *IEEE Trans. Power Electron.*, vol. 33, no. 5, pp. 4362–4372, May 2018.
[48] D. Youla, L. Castriota, and H. Carlin, "Bounded real scattering matrices and the foundations of linear passive network theory," *IRE Trans. Circuit Theory*, vol. 6, no. 1, pp. 102–124, Mar. 1959.
[49] A. J. van der Schaft, *L2-Gain and Passivity Techniques in Nonlinear Control*, vol. 2. London, U.K.: Springer, 2000.
[50] H. K. Khalil and J. Grizzle, *Nonlinear Systems*, vol. 3. Upper Saddle River, NJ, USA: Prentice-Hall, 2002.

MUSTAFA ALRAYAH HASSAN (Member, IEEE) received the B.Sc. degree in electrical engineering from the University of Blue Nile, Ad-Damazin, Sudan, in 2006, the M.Sc. degree in electrical power engineering from the University of Khartoum, Khartoum, Sudan, in 2013, and the Ph.D. degree in electrical engineering from the Hebei University of Technology, Tianjin, China, in 2019.

He worked as a Lecturer with the International University of Africa, Khartoum, in 2014. Since 2019, he has been a Visiting Assistant Professor with the African Center of Excellence in Energy for Sustainable Development, University of Rwanda, Kigali, Rwanda. He is currently a Postdoctoral Researcher with Wuhan University, Wuhan, China. He is also an Assistant Professor with the University of Blue Nile. He has authored or coauthored many conferences and journal articles. He reviewed many articles with several IEEE journals such as the IEEE TRANSACTIONS ON INDUSTRIAL ELECTRONICS, the IEEE JOURNAL OF EMERGING AND SELECTED TOPICS IN POWER ELECTRONICS, IEEE ACCESS, and *IET Power Electronics*. His current research interests include, power electronic converters, distributed generation systems, smart grid, DC microgrids stability and control, health management of dc-dc power converters in HVDC Grids, nonlinear control, adaptive passivity-based control, and sliding mode control.

YIGANG HE received the M.Sc. degree in electrical engineering from Hunan University, Changsha, China, in 1992, and the Ph.D. degree in electrical engineering from Xi'an Jiaotong University, Xi'an, China, in 1996.

In 1990, he joined the College of Electrical and Information Engineering, Hunan University and was promoted to an Associate Professor, a Professor in 1996 and 1999, respectively. From 2006 to 2011, he worked as the Director of the Institute of Testing Technology for Circuits and Systems, Hunan University. He was a Senior Visiting Scholar with the University of Hertfordshire, Hatfield, U.K., in 2002. From 2011 to 2017, he worked as the Head of School of Electrical Engineering and Automation, Hefei University of Technology. In December 1, 2017, he joined Wuhan University, China. He is currently the Vice-Head of School of Electrical Engineering and Automation, Wuhan University. Meanwhile he was the Vice President of the China's Energy Institute of Science and Technology, the Vice President of Anhui Scientists Entrepreneurs Association, the Director of the State Local Joint Engineering Laboratory for renewable energy grid technology. His teaching and research interests are in the areas of power electronic circuit theory and its applications, testing and fault diagnosis of analog and mixed-signal circuits, electrical signal detection, smart grid, satellite communication monitoring, and intelligent signal processing. On the above research areas, he has presided over a number of state-level projects research such as the National Natural Science Foundation of China, the State Key Program of National Natural Science Foundation of China, the National Key Research and Development Plan of important scientific instruments and equipment development, the National High Technology Research and Development Program of China, the Major State Basic Research Development Program of China, etc. He has published some 300 journal and conference papers which was included more than 1000 times in Science Citation Index of American Institute for Scientific Information in the aforementioned areas and several chapters in edited books.

Dr. He has been the General Chair, the Session Chair, and the Committee Member of a lot of international academic conferences respectively. He was a recipient of a number of national and international awards, prizes, and honors. For example, he was the winner of National Outstanding Youth Science Fund, the China National Excellent Science and Technology Worker.